Fat/Water Separation in a Single MRI Image with Arbitrary Phase Shift

M. Dylan Tisdall and M. Stella Atkins

Computing Science, Simon Fraser University, Burnaby, BC, Canada

ABSTRACT

Signal from fat is normally removed from MR images either by fat separation techniques that distinguish water from fat signal after the data has been received, or by fat suppression techniques that prevent the fat signal from being received. Most approaches to fat separation are variations on Dixon imaging. The primary downside to Dixon imaging is the requirement for multiple images with stationary anatomy, often with specific TEs. An alternate approach is to take only one image, estimate phase errors to correct for inhomogeneity or other effects, and then separate the water and fat using the known phase shift. This has shown promise in previously published work, but the water and fat signals were always perpendicular, requiring a fixed TE. We consider the possibility of separation from a single, phase-corrected image with an arbitrary angle between water and fat signals. We note that a change of basis will separate water and fat signals into two images with additive zero-mean Gaussian noise. However, as the angle between water and fat nears pi or 0, the noise power in the separated images increases rapidly. We discuss techniques for reducing this noise magnification.

Keywords: Magnetic resonance imaging, Fat separation, Phase error estimation, Denoising, Dixon imaging

1. INTRODUCTION

The ^{1}H NMR spectrum of human anatomy is often simplified as two significant peaks. The first of these, ω_w at approximately $B_0 \times 42.57$MHz/T, is from water while the second peak, ω_f approximately 3.5 ppm higher, is produced by lipids. It is often desired that an MR image contain only the water signal, particularly in situations where fatty tissues may appear brightly and obscure fine anatomical structures. This filtering is normally achieved using one of two families of techniques that rely on specific pulse sequences and/or post-processing. The fat suppression techniques use pulse sequences designed to prevent the reception of signal from fatty tissue. The alternative, fat separation techniques attempt to produce two images (water and fat) after the data has been acquired. The most well-known fat separation approaches are based Dixon imaging, the majority of which require three or more images of static anatomy at different TEs. Normally, the TE values are fixed so that the fat and water images can be distinguished.[1, 2]

The requirement for multiple images of fixed anatomy limit the use of Dixon imaging to static anatomy and require care in minimizing patient motion. Additionally, the demand for three times more images than a regular scan necessitates a similar increase in acquisition time. Finally, the requirement of fixed TE reduces the available scanning parameters.

Recently, a fat separation process has been proposed that requires multiple calibration scans, but afterwards can produce separate fat and water images from single data acquisitions.[3] This technique promises the ability to record images with higher spatial and temporal resolution than the multi-image Dixon techniques. However, the TE in the proposed system is fixed so that the phase shift of fat relative to water is $(1/2 + k)\pi$ where $k \in \mathbb{Z}$. Thus, while the new technique has reduced the number of acquisitions required, the issue of fixed TE is still present.

In this paper, we consider the effects of relaxing this restriction and present some initial simulation results to illustrate our analysis. In Sect. 2 we provide a brief explanation of the principle of phase error estimation

Further author information: (Send correspondence to M.D.T.)
M.D.T.: E-mail: mtisdall@cs.sfu.ca, Telephone: 1 604 291 5509
M.S.A.: E-mail: stella@cs.sfu.ca, Telephone: 1 604 291 4288

Medical Imaging 2006: Physics of Medical Imaging, edited by Michael J. Flynn, Jiang Hsieh,
Proceedings of SPIE Vol. 6142, 61423X, (2006) · 1605-7422/06/$15 · doi: 10.1117/12.655128

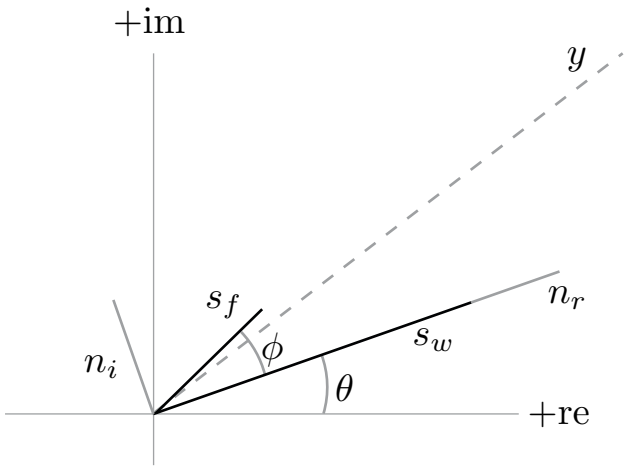

Figure 1. The components of a single complex-valued pixel. The black vectors s_w and s_f are the signal from water and fat respectively. ϕ is the angle between water and fat. θ is the phase error. The grey vectors n_r and n_i are the real and imaginary noises respectively, although they do not fall along the real and imaginary axes because of the phase error. The dashed vector, y, is the recorded value for the pixel.

and its use in fat separation. In Sect. 3 we use this model to present an analysis of the effects of altering the TE, particularly regarding noise in the separated images, . We consider the use of the maximum likelihood estimator (MLE) to reduce noise in the final images, and discuss the limitations of this approach in Sect. 4. Our conclusions and discussion of future work are presented in Sect. 5.

2. FAT SEPARATION VIA PHASE ERROR ESTIMATION

MR images are initially complex-valued and are normally converted to greyscale intensities by taking the magnitude of each pixel. For our purposes, we can describe the recorded MRI pixels as a complex-valued vector, $\boldsymbol{y}$, defined by

$$\boldsymbol{y}[x] = (\boldsymbol{s_w}[x] + \boldsymbol{s_f}[x]\exp(\mathrm{i}\,\phi) + \boldsymbol{n_r}[x] + \mathrm{i}\,\boldsymbol{n_i}[x])\exp(\mathrm{i}\,\boldsymbol{\theta}[x])\,, \tag{1}$$

where x is the index of a pixel in the image, $\boldsymbol{s_w}$ and $\boldsymbol{s_f}$ are the real-valued vectors of signal from water and fat respectively, ϕ is the angle between water and fat determined by scan parameters, $\boldsymbol{n_r}$ and $\boldsymbol{n_i}$ are vectors of samples from an additive white Gaussian noise (AWGN) with variance σ^2, and $\boldsymbol{\theta}$ is the phase error. The relationships of these quantities are shown in Fig. 1.

Spin echo and similar pulse sequences are normally implemented so that $\phi = 0$, water and fat magnitudes are summed, and the phase of each $\boldsymbol{y}[x]$ is determined by the noise and $\boldsymbol{\theta}$. However, in the pulse sequences used for fat separation, it is usual to delay or advance the recording by some period, τ. For example, the TE of a spin echo pulse sequence at 1.5 T is the point when water and fat signals are in phase. It is normally the case that the TE of this sequence occurs in the middle of the read-out direction sampling and so $\phi = 0$. If, however, the commencement of the readout gradient's application is delayed by τ, the acquired image will have $\phi = (\omega_f - \omega_w)\tau$. Similarly, in a gradient echo sequence, we have $\phi = (\omega_f - \omega_w)\mathrm{TE}$.

Algorithms have been developed for estimating $\boldsymbol{\theta}$ in a variety of different pulse sequences.[3–5] For this paper, we will assume that an appropriate pulse sequence and algorithm can be employed to closely estimate $\boldsymbol{\theta}$ in a pulse sequence where ϕ is known and non-zero. Given this estimate, a dephased image, $\boldsymbol{y'}$, can be defined by multiplying equation (1) with the estimated phasor, giving

$$\boldsymbol{y'}[x] = \boldsymbol{y}[x]\exp(\mathrm{i}\,\boldsymbol{\theta}[x]) = \boldsymbol{s_w}[x] + \boldsymbol{s_f}[x]\exp(\mathrm{i}\,\phi) + \boldsymbol{n_r}[x] + \mathrm{i}\,\boldsymbol{n_i}[x]\,. \tag{2}$$

In order to simplify our future equations, we will rewrite our complex variables as 2D vectors in the basis $\{1,0\},\{0,\mathrm{i}\}$. Thus, equation (2) can be rewritten as

$$\boldsymbol{y'} = \boldsymbol{s_w}\{1,0\} + \boldsymbol{s_f}\{\cos\phi,\sin\phi\} + \boldsymbol{n_r}\{1,0\} + \boldsymbol{n_i}\{0,1\}\,. \tag{3}$$

We noted that in previous work ϕ was fixed so that $\{\cos\phi, \sin\phi\} = \{0, 1\}$ or $\{0, -1\}$. In this case, a water image can be recovered by taking $\boldsymbol{y'_w} = \boldsymbol{y'}\{1, 0\}^{\mathrm{T}}$ and a fat image can be recovered by taking $\boldsymbol{y'_f} = \boldsymbol{y'}\{0, 1\}^{\mathrm{T}}$ and inverting the sign of the fat pixels if necessary. In the complex-valued pixel notation, this is equivalent to simply taking the real (water) and imaginary (fat) components of each pixel.[3] Additionally, we know that $\boldsymbol{n_r}$ will be summed with the water image and $\boldsymbol{n_i}$ will be summed with the fat image. Thus, both images will have AWGN with variance σ^2.

3. EFFECTS OF VARYING TE

Fortunately, it is not much more complicated to extend this idea to almost any ϕ value and thus an arbitrary TE. Again, let us think of the recorded 2D pixels in $\boldsymbol{y'}$ as being in a real/imaginary basis. We will restrict ourselves to cases where $\phi \neq 0, \pi$ to ensure that fat and water signals are linearly independent. Barring this restriction, converting to a basis where water and fat are orthogonal (we will call this the water/fat basis for convenience) requires multiplication with the matrix

$$\mathbf{P} = \begin{bmatrix} 1 & -\cot\phi \\ 0 & \csc\phi \end{bmatrix}.$$

Performing this change of basis on equation (3) gives

$$\begin{aligned} \mathbf{P}\boldsymbol{y'}^{\mathrm{T}} &= \mathbf{P}(\boldsymbol{s_w}\{1,0\})^{\mathrm{T}} + \mathbf{P}(\boldsymbol{s_f}\{\cos\phi, \sin\phi\})^{\mathrm{T}} + \mathbf{P}(\boldsymbol{n_r}\{1,0\})^{\mathrm{T}} + \mathbf{P}(\boldsymbol{n_i}\{0,1\})^{\mathrm{T}} \\ &= (\boldsymbol{s_w}\{1,0\})^{\mathrm{T}} + (\boldsymbol{s_f}\{0,1\})^{\mathrm{T}} + (\boldsymbol{n_r}\{1,0\})^{\mathrm{T}} + (\boldsymbol{n_i}\{-\cot\phi, \csc\phi\})^{\mathrm{T}}. \end{aligned} \tag{4}$$

To recover a water image with a known ϕ, we can use $\boldsymbol{y'_w} = (\mathbf{P}\boldsymbol{y'}^{\mathrm{T}})^{\mathrm{T}}\{1,0\}^{\mathrm{T}}$ and similarly $\boldsymbol{y'_f} = (\mathbf{P}\boldsymbol{y'}^{\mathrm{T}})^{\mathrm{T}}\{0,1\}^{\mathrm{T}}$ will produce the fat image. Substituting these back into equation (4), we have the water image and fat images

$$\begin{aligned} \boldsymbol{y'_w} &= \boldsymbol{s_w} + \boldsymbol{n_r} - (\cot\phi)\boldsymbol{n_i} \\ \boldsymbol{y'_f} &= \boldsymbol{s_f} + (\csc\phi)\boldsymbol{n_i}. \end{aligned} \tag{5}$$

Since we know that $\boldsymbol{n_r}$ and $\boldsymbol{n_i}$ are independent and both have variance σ^2, we can rewrite $\boldsymbol{n_r} - (\cot\phi)\boldsymbol{n_i}$ as the vector $\boldsymbol{n_w}$ of samples from an AWGN with variance $(\csc\phi)^2\sigma^2$. Similarly, we can replace $(\csc\phi)\boldsymbol{n_i}$ with vector $\boldsymbol{n_f}$ of samples from an AWGN with variance $(\csc\phi)^2\sigma^2$. Note that the covariance of $\boldsymbol{n_w}[x]$ and $\boldsymbol{n_f}[x]$ is given by

$$\begin{aligned} \mathrm{cov}(\boldsymbol{n_w}[x], \boldsymbol{n_f}[x]) &= \mathrm{cov}(\boldsymbol{n_r}[x] - (\cot\phi)\boldsymbol{n_i}[x], (\csc\phi)\boldsymbol{n_i}[x]) \\ &= \mathrm{cov}(\boldsymbol{n_r}[x], (\csc\phi)\boldsymbol{n_i}[x]) - \mathrm{cov}((\cot\phi)\boldsymbol{n_i}[x], (\csc\phi)\boldsymbol{n_i}[x]) \\ &= -(\cot\phi)(\csc\phi)\sigma^2 \end{aligned} \tag{6}$$

Although they have non-zero covariance, both the fat and water images will each contain only their own signal and have equal power AWGN regardless of ϕ. The orthogonal case laid out in Sect. 2 is a particular case where $(\csc\phi)^2 = 1$ and so the noise variance is not altered and the fat and fat and water image noises are independent. Since we have shown that water and fat signals can be separated as long as they are linearly independent, the remaining concern is with the signal to noise ratio (SNR) of the resulting images. We have seen that in the case where $\phi = (1/2 + k)\pi$, the SNR in a water or fat pixel is $\boldsymbol{s_w}[x]/\sigma$ and $\boldsymbol{s_f}[x]/\sigma$ respectively. The relative SNR of the same pixel given an arbitrary ϕ compared to the orthogonal case is simply $\frac{1}{|\csc\phi|}$. Thus, as can be seen in Fig. 2, the SNR of an image is halved relative to the orthogonal case by picking a shorter TE and thus setting $\phi = \pi/6$. This illustrates that in a situation with sufficiently high SNR, it is quite feasible to vary the TE and still produce acceptable images.

4. MAXIMUM LIKELIHOOD ESTIMATOR FOR REDUCING NOISE

4.1. Domain-specific constraints and estimator

While a change of basis will separate the water and fat components of an MR image, we have seen that there is a significant decrease in SNR once ϕ varies far from the orthogonal case. In previous work with phase-corrected

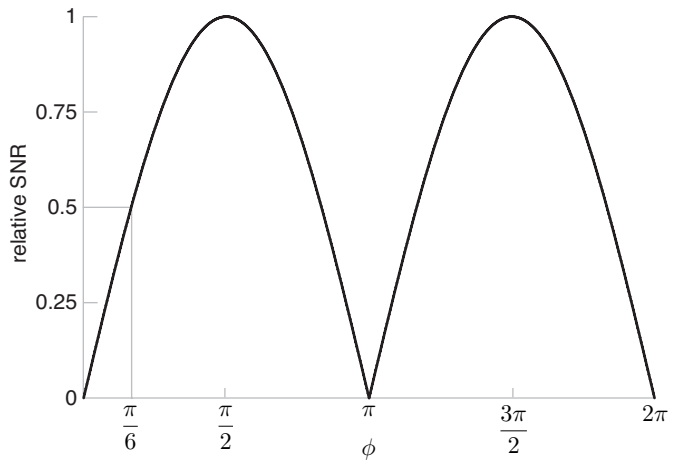

Figure 2. Relative SNR of a pixel with arbitrary ϕ in a separated water or fat image compared to the case where $\phi = (1/2 + k)\pi$. The curve shows the trade-off between varying TE and the decrease in resulting SNR.

images, we noted that by using the ML estimate for each pixel, we could improve SNR.[5] In particular, we fixed $\phi = 0$ and noted that $\boldsymbol{s_w}$ and $\boldsymbol{s_f}$ must contain only non-negative entries. Thus the MLE in this limited case consisted of the the non-negative, real component of each pixel.

In our current problem, we still know that $\boldsymbol{s_w}$ and $\boldsymbol{s_f}$ are non-negative, but there are several additional complications. The MLE can be thought of as being the estimator that forces our signal estimates to be in the valid (i.e., non-negative) range while assuming the minimum amount of noise in the recorded values.[6] The first decision is whether we are better determining the MLE before or after the change of basis. Though the two are equivalent, we have chosen to calculate the MLE before the change of basis because $\mathbf{P}$ does not necessarily produce a circular noise distribution in the water/fat basis (see Appendix A). This is the reason why equation (6) shows non-zero covariance. By operating in the real/imaginary basis, where the noise variance is equal in all directions and orthogonal noise samples are independent, we produce a clearer set of calculations that are more consistent regardless of ϕ.

Our approach to using the MLE for noise reduction will consist of two steps. First, we will use the MLE to produce an estimate in the real/imaginary basis of the true water and fat signals in each pixel. Then, we will multiply by $\mathbf{P}$ to convert the estimated values to the water/fat basis for separation. Intuitively, the goal of this two-step approach is to minimize the amount of noise in the pixels before the change of basis, so that the amplifying effects $\mathbf{P}$ are not as visible.

The valid range of estimates for the true signal in the real/imaginary basis is produced by using non-negative values of a and b in, $a\{1, 0\} + b\{\cos\phi, \sin\phi\}$. As can be seen in Fig. 3 these vectors describe a cone in $\mathbb{R}^2$. If a pixel is inside this cone, the ML estimate of the true signal is the current pixel value. If the pixel is outside this cone, the estimate of the true signal is the nearest point on the surface of the cone.

In the speical case where water and fat are orthogonal ($\phi = k\pi/2$), the cone is either the first or fourth quadrant of $\mathbb{R}^2$, depending on whether k is odd or even. In this case, the ML estimate in the real/imaginary basis is essentially the same as the estimate in the water/fat basis as there is no noise correlation between the images and they can be denoised individually with the single-image technique we previously described.[5]

Our algorithm for implementing the MLE is as follows:

1. Calculate $\mathbf{P}\boldsymbol{y'}^{\mathrm{T}}$ to determine the initial estimates for each pixel in the water/fat basis
2. For each pixel, $\{a, b\}$ in the water/fat basis, if $a, b \geq 0$, then let the real/imaginary estimate of this pixel be the recorded value.

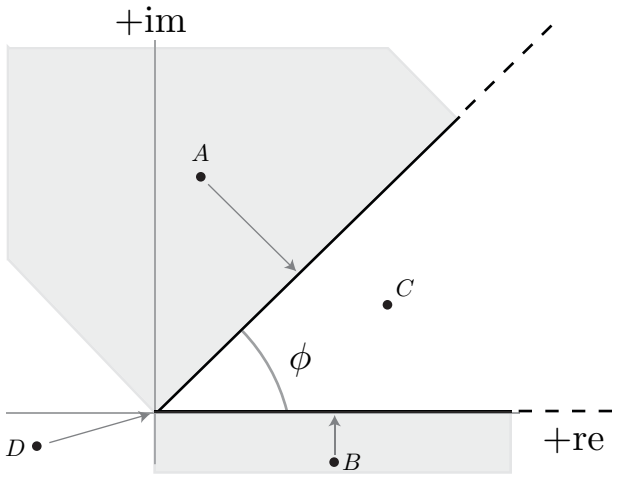

Figure 3. Illustration of the MLE for true signal in the real/imaginary basis. The two grey regions represent areas where pixels are projected onto either the fat boundary of the cone (top region in this figure) or water boundary (bottom region). Point A is not valid because it has negative water component in the water/fat basis. The MLE will locate the estimated true signal for this pixel on the fat boundary. Point B is not valid because it has negative fat component in the water/fat basis. The estimate is on the water boundary by the MLE. Point C is inside the cone and so is a valid estimate of the true signal. Point D is nearer to the origin that to either of the non-negative boundaries, and so the ML estimate for this pixel is zero signal from either water or fat.

3. For each pixel in wich $a < 0$ or $b < 0$, project the recorded real/imaginary vector onto $\{1, 0\}$ and $\{\cos\phi, \sin\phi\}$. Set the estimate to the nearest of these two projections. If this estimate produces a negative a or b, then the correct estimate is $\{0, 0\}$ in the real/imaginary basis.

4. Multiply the real/imaginary ML estimates by $\mathbf{P}$ to produce the ML estimates in the water/fat basis.

Examples of synthetic fat and water signals separated with and without the MLE are shown in Fig. 4.

4.2. Ghosting with MLE

The examples shown in Fig. 4 highlight the ghosting problem that arises with the use of the MLE to reduce noise. While noise is clearly reduced in some areas of the image, the MLE does not produce constant noise variance in all pixels of the water or fat images. In particular, we note that pixels with a high estimated water signal have higher noise power in the fat image and vice versa. We will show the strength of these ghosts is a function of ϕ and results from the cone shape of the valid region for true signal estimates.

We will concern ourselves with $0 < \phi < \pi/2$ as other cases can, for the most part, be generalized from this one. To make clear how the ghost in Fig. 4 g is produced, let us consider the case of a pixel with water signal a and no fat signal. By equation (5) we know that noise in the real direction does not appear in the fat image. Noting this, to simplify our model we will assume the real-noise is negligible compared to a and so ignore its effects. Thus, noise in the imaginary direction will be considered as the sole noise in the system. Given these simplifying assumptions, the PDF for the ML estimate of fat intensity, b, in this pixel is

$$f(b) = \begin{cases} \int_{-\infty}^{0} \frac{1}{\sqrt{2\pi}\sigma} \exp\left(-\frac{y^2}{2\sigma^2}\right) dy & \text{if } b = 0 \\ \frac{1}{\sqrt{2\pi}\sigma} \exp\left(-\frac{(b\sin\phi)^2}{2\sigma^2}\right) \sin\phi & \text{if } b \le a\cos\phi \\ \frac{1}{\sqrt{2\pi}\sigma} \exp\left(-\frac{(b-a\cos\phi)^2}{2(\sigma\sin\phi)^2}\right) \frac{1}{\sin\phi} & \text{if } b > a\cos\phi \\ 0 & \text{if } b < 0 \end{cases}.$$

Considering this equation, and returning to Fig. 3, we see that as a increases, the width across the cone in the imaginary direction from point $\{a, 0\}$ also increases. Additionally, we know that the MLE takes any point inside

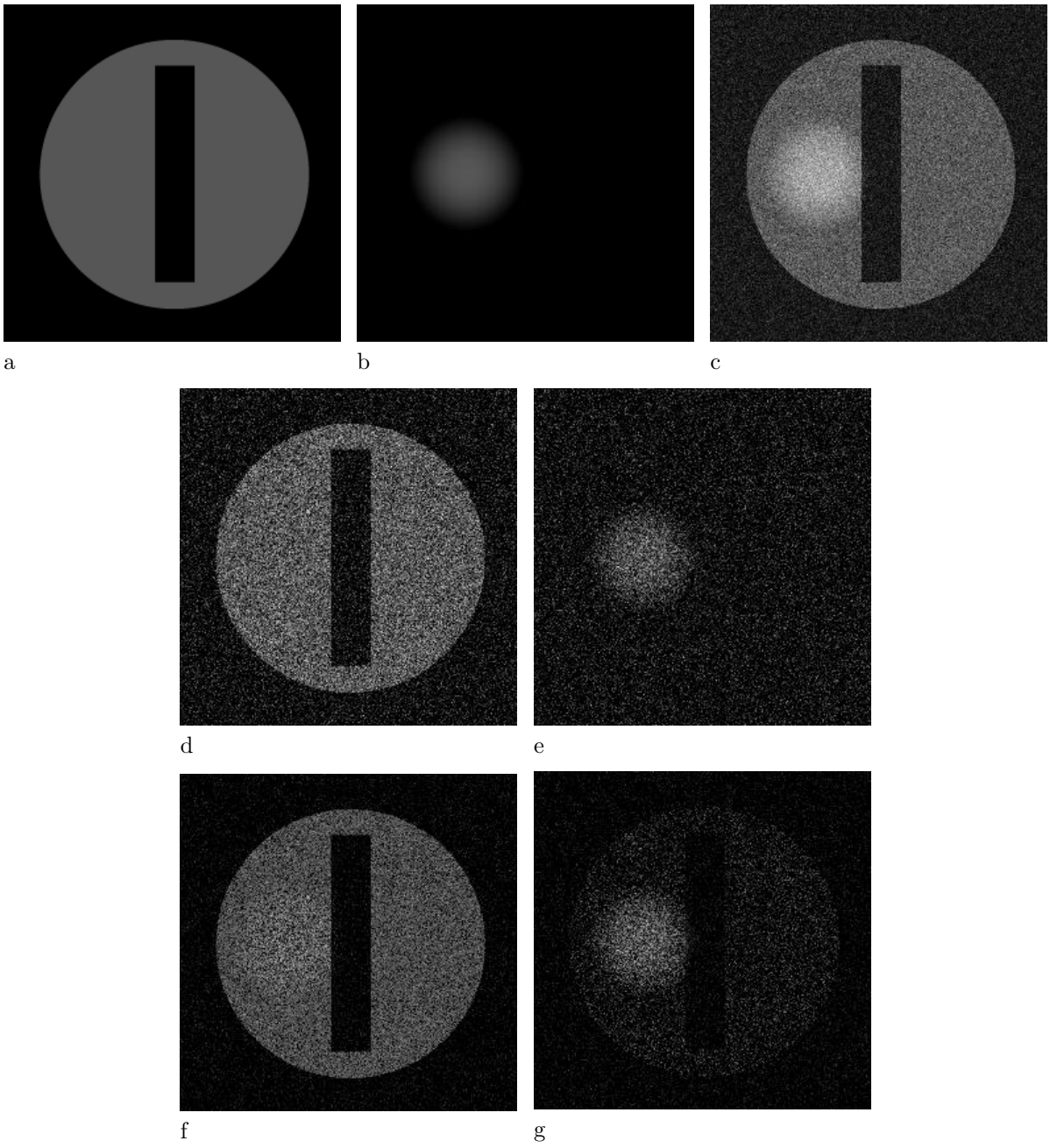

Figure 4. Example of fat/water separation with $\phi = \pi/6$. All images are shown with the same window width and center. The true water and fat signals (peak value = 1) are shown in a and b respectively. The magnitude image with $\sigma = 0.25$ is shown in c. Images d and e are the water and fat images reconstructed by multiplication with $\mathbf{P}$. Note the doubling of noise power visible in these images. The MLE water and fat images are shown in f and g. Note the ghosting effect of the MLE, particularly the water ghost in image g.

the cone as the estimate of the true signal. While the noise variance in the imaginary direction does not vary with a, the ghosting effect in fat images occurs because it is more likely that a noisy value will fall inside the width of the cone and be accepted as the ML estimate. The significance of a noisy value falling inside the cone is that if the noisy value is beyond the fat boundary in the imaginary direction, the MLE discards some of the noise by moving it 'backwards' onto the boundary (see point A in Fig. 3). Thus, in regions with low a most of the imaginary noise is rejected but in areas with large a, a significant portion is included in the estimate, giving the impression of a water ghost in the fat image.

Similar derivations can be performed to show the ghosting effect of bright fat signals in the water image.

5. CONCLUSIONS

Previous work on water/fat separation has shown the possibility of producing water and fat images from a single acquisition. However, in these proposals the TE was fixed to make water and fat signals orthogonal. We have shown that it is not necessary to fix the TE and that a simple matrix multiplication is sufficient to reconstruct an image with non-orthgonal fat and water signals. We have also analyzed the effects of this matrix multiplication on the SNR of the water and fat images and presented a simple equation for determining the relative SNR of acquisition different TEs. We show that, given sufficient initial SNR, it is quite feasible to vary TE significantly and still separate fat and water signals.

In an attempt to improve the SNR of the water and fat images, we used the MLE to filter noise from the images. While the MLE works well for this task in the case of parallel or perpendicular fat and water signals, we noted a ghosting effect at all intermediate angles. These ghosts are caused by noise being included in the ML estimate and so are made brighter in proportion to all other noise effects as the relative SNR decreases. Based on these results, a better estimator for true signal must be investigated.

Finally, we would like to begin testing this separation technique on clinical data to determine what sort of practical issues arise that have not be accounted for in our relatively simple model of the acquisition process.

APPENDIX A. SINGULAR VALUE DECOMPOSITION OF CHANGE OF BASIS MATRIX

In the real/imaginary basis, the 2D AWGN represented by $\boldsymbol{n_r}\{1,0\} + \boldsymbol{n_i}\{0,1\}$ is a circular distribution since both $\boldsymbol{n_r}$ and $\boldsymbol{n_i}$ have variance σ^2. The singular value decomposition (SVD) of $\mathbf{P}$ can be used to describe the effects of $\mathbf{P}$ on this circle and provide further insight into the effects of $\mathbf{P}$ on the noise distribution.

We first find the eigenvalues of $\mathbf{P}^{\mathrm{T}}\mathbf{P}$ via the characteristic equation and get,

$$\lambda = \csc^2\phi \pm |\cot\phi \csc\phi| \,. \tag{7}$$

This gives the singular values of $\mathbf{P}$ as $s_1 = \sqrt{\csc^2\phi + |\cot\phi\csc\phi|}$ and $s_2 = \sqrt{\csc^2\phi - |\cot\phi\csc\phi|}$.

With the eigenvalues we determined in equation (7), we can find the eigenvectors using

$$\begin{bmatrix} 1 - \csc^2\phi \mp |\cot\phi\csc\phi| & -\cot\phi \\ -\cot\phi & \cot^2\phi + \mp|\cot\phi\csc\phi| \end{bmatrix} \begin{bmatrix} x_1 \\ x_2 \end{bmatrix} = 0 \,.$$

This gives the unit-length eigenvectors

$$\boldsymbol{x} = \frac{1}{\sqrt{2\csc^2\phi \mp 2|\cot\phi\csc\phi|}} \left[\cot\phi \mp |\cot\phi\csc\phi|\tan\phi, 1\right]^{\mathrm{T}} \,.$$

These eigenvectors are also the right singular vectors of $\mathbf{P}$, in the order

$$\begin{aligned} \boldsymbol{v}_1 &= \frac{1}{\sqrt{2\csc^2\phi - 2|\cot\phi\csc\phi|}} \left[\cot\phi - |\cot\phi\csc\phi|\tan\phi, 1\right]^{\mathrm{T}} \\ \boldsymbol{v}_2 &= \frac{1}{\sqrt{2\csc^2\phi + 2|\cot\phi\csc\phi|}} \left[\cot\phi + |\cot\phi\csc\phi|\tan\phi, 1\right]^{\mathrm{T}} \,. \end{aligned}$$

It is useful to note that $\boldsymbol{v}_1 \cdot \boldsymbol{v}_2 = 0$. Since the right singular vectors represent the direction of sampling in our 2D AWGN, we see that $\mathbf{P}$ transforms the noise by taking two perpendicular samples. Since the samples are perpendicular, they will be independent 1D AWGN samples with variance σ^2.

Lastly, we need to solve for the left singular vectors of $\mathbf{P}$ to determine the alignment of the noise samples in water/fat space. To do this, we solve

$$\boldsymbol{u}_i = \frac{1}{s_i}\mathbf{P}\boldsymbol{v}_i\,.$$

Simplify the result gives

$$\begin{aligned}\boldsymbol{u}_1 &= \left[-\frac{|\cot\phi\csc\phi|\tan\phi}{\sqrt{2}|\csc\phi|}, \frac{\csc\phi}{\sqrt{2}|\csc\phi|}\right]^{\mathrm{T}} \\ \boldsymbol{u}_2 &= \left[\frac{|\cot\phi\csc\phi|\tan\phi}{\sqrt{2}|\csc\phi|}, \frac{\csc\phi}{\sqrt{2}|\csc\phi|}\right]^{\mathrm{T}}.\end{aligned}$$

We can simplify this further by noting that if $\phi \neq k\pi/2$ (i.e., if water and fat signals are linearly independent and not orthogonal) then we have

$$\frac{\csc\phi}{|\csc\phi|} = \begin{cases}1 & \text{if } 2n\pi < \phi < (2n+1)\pi, n \in \mathbb{Z} \\ -1 & \text{if } (2n-1)\pi < \phi < 2n\pi, n \in \mathbb{Z}\,,\end{cases}$$

and

$$\frac{|\cot\phi\csc\phi|\tan\phi}{|\csc\phi|} = \begin{cases}1 & \text{if } (2n-\frac{1}{2})\pi < \phi < (2n+\frac{1}{2})\pi, n \in \mathbb{Z} \\ -1 & \text{if } (2n+\frac{1}{2})\pi < \phi < (2n+\frac{3}{2})\pi, n \in \mathbb{Z}\,.\end{cases}$$

Thus we find that $\boldsymbol{u}_1$ and $\boldsymbol{u}_2$ will be unit length, perpendicular, and aligned diagonally between the water and fat axes.

Putting together the results from the SVD of $\mathbf{P}$, we see that, given a real/imaginary image with 2D AWGN, the resulting water/fat image with have a noise distribution shaped like an ellipse oriented diagonally to the water and fat axes. The major axis of the ellipse will have noise variance $s_1^2\sigma^2$ and the minor axis will have $s_2^2\sigma^2$. Since the ellipse is diagonal between the bases, its projection onto either axis, and thus its contribution to the water and fat images, will be a 1D AWGN with equal power in both directions as derived in Sect 3.

ACKNOWLEDGMENTS

The authors would like to thank the National Science and Engineering Research Council for their support of this research.

REFERENCES

1. W. T. Dixon, "Simple proton spectroscopic imaging," *Radiology* **153**, pp. 189–194, 1984.
2. G. H. Glover, "Multipoint dixon technique for water and fat proton and susceptibility imaging," *J. Magn. Reson. Im.* **1**, pp. 521–530, 1991.
3. H. Yu, C. A. McKenzie, A. Shimakawa, A. C. Brau, A. R. Pineda, N. J. Pelc, J. H. Brittain, and S. B. Reeder, "Parallel imaging accelerated single acquisition water-fat separation for dynamic imaging," in *Proc. ISMRM*, **13**, 2005.
4. D. Noll, D. Nishimura, and A. Macovski, "Homodyne detection in magnetic resonance imaging," *IEEE Trans. Med. Imag.* **10**, pp. 154–163, 1991.
5. D. Tisdall and M. S. Atkins, "MRI denoising via phase error estimation," in *Proc. SPIE*, **5747**, pp. 646–654, 2005.
6. D. Middleton, *An Introduction to Statistical Communication Theory*, McGraw Hill, 1960.